Available online at www.sciencedirect.com
SCIENCE DIRECT
Journal of Catalysis 233 (2005) 388–398
JOURNAL OF CATALYSIS
www.elsevier.com/locate/jcat

Effect of phosphorous modifier on V_2O_5/TiO_2 catalyst: ODH of propane

Rudra Pratap Singh [a], Miguel A. Bañares [b], Goutam Deo [a,*]

[a] *Department of Chemical Engineering, Indian Institute of Technolgoy Kanpur, Kanpur 208 016, India*
[b] *Instituto de Catálisis y Petroleoquímica, CSIC, Campus Cantoblanco, E-28049, Madrid, Spain*

Received 10 March 2005; revised 10 May 2005; accepted 13 May 2005

Available online 13 June 2005

Abstract

The effect of the P/V ratio on the structure, properties, and reactivity of titania-supported vanadia is evaluated. The Raman spectra and temperature-programmed reduction studies reveal a progressive P–V interaction with increasing P/V ratio until nanoscaled α_I-$VOPO_4$ forms above a monolayer. Propane oxidative dehydrogenation (ODH) studies reveal that the conversion and selectivities of the catalysts strongly depend on the P–V interaction. For a Mars–van Krevelen model, kinetic parameters are successfully estimated by minimization of an objective function with the use of a genetic algorithm. With an increase in the P/V ratio the kinetic parameters reveal a progressive decrease in the primary ODH reaction rate constant and in the rate constant ratio for propene degradation to propene formation. The decrease in the rate constant ratio for propene degradation and propene formation with increasing P/V ratio leads to a more efficient catalyst. Thus, with the proper design of the catalyst the propene yield can be increased.
© 2005 Elsevier Inc. All rights reserved.

Keywords: Metal oxide; Supported catalysts; Vanadia; Phosphorous; Titania; Propane yield; Raman; TPR

1. Introduction

The oxidative dehydrogenation (ODH) of propane (C_3H_8) to propene (C_3H_6) is an attractive alternative to the classic catalytic dehydrogenation process. Several of the drawbacks associated with the classic process can be overcome with the ODH process, provided a proper catalyst is developed that maximizes propene yield and the reactor is operated away from the explosive limits.

The activation of the stable C–H bond of propane at a low temperature combined with protection of the formed propene from subsequent overoxidation is a prerequisite for a catalyst to be successful in the process. Among the catalysts that have been developed, vanadia-containing catalysts are some of the more active and selective ones for the ODH of propane [1]. They have been widely used as an active component in mixed oxides and on supports for the ODH of propane. Supported vanadium oxide has gained much importance over other catalysts because of its high performance, better thermal stability, and larger surface area [2–5]. Usually, an inverse relation between the conversion and propene selectivity is observed for the propane ODH reaction. Consequently, the propene yield is limited. To tune the inverse relationship between conversion and selectivity, we considered several factors.

The propane ODH reaction can be visualized as a network of reactions as shown in Scheme 1 [6]. This scheme is a network of reactions that gives rise to primary, secondary, and tertiary products and only addresses the state of carbon. For example, carbon dioxide (CO_2) is produced as a primary product from propane (C_3H_8), a secondary product from propene (C_3H_6), or a tertiary product from carbon monoxide (CO); and C_3H_6 can only be produced as a primary product of propene. Carbon deposition is not considered since it is insignificant under the conditions commonly used.

The above reaction scheme can be further simplified, assuming that C_3H_6 is the only primary product and the tertiary reaction of CO_2 formation from CO is neglected. With these simplifications the reaction is essentially a consecutive

* Corresponding author. Fax: +91 512 2590104.
E-mail address: goutam@iitk.ac.in (G. Deo).

0021-9517/$ – see front matter © 2005 Elsevier Inc. All rights reserved.
doi:10.1016/j.jcat.2005.05.010

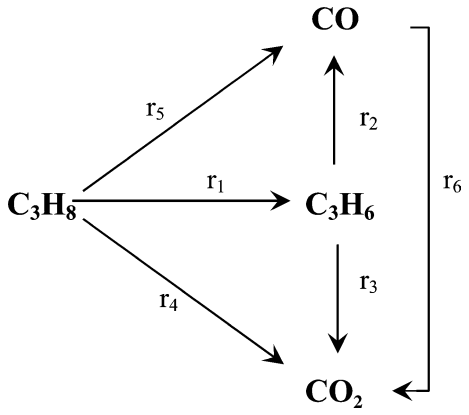

Scheme 1. Generalized reaction scheme for propane ODH.

reaction with propene as the primary product and the carbon oxides (CO_x) as the secondary products. Lumping together of CO_x formation, however, is not straightforward and depends on the activation energy differences of CO and CO_2 formation from propene. Optimization of propene yields thus becomes a classical textbook problem where the intermediate or C_3H_6 yield requires optimization, with the added complication of having two independent secondary products instead of one [7].

For a simple first-order reaction scheme, where C_3H_6 is the only primary product formed and CO and CO_2 are independent secondary products, optimization of C_3H_6 yield strongly depends on the ratio of the rate constants, $(k_2+k_3)/k_1$, where k_1 is the rate constant for the primary C_3H_6 formation reaction, k_2 is the rate constant for CO formation, and k_3 is the rate constant for CO_2 formation. Consequently, the optimization of C_3H_6 yield requires minimization of the $(k_2+k_3)/k_1$ ratio, which depends on the operating conditions (partial pressures and temperature) and the catalyst. For example, for different activation energies an increase in temperature changes the $(k_2+k_3)/k_1$ ratio, since the rate constants are a function of temperature. Usually for the propane ODH reaction the activation energies of formation of the primary (C_3H_6) and secondary products are different. Furthermore, changing the catalyst can change the $(k_2+k_3)/k_1$ ratio by changing the pre-exponential factor if the activation energies of formation of the primary and secondary products are invariant. This concept of changing the ratio of the rate constants with temperature and catalysts to increase the C_3H_6 yield has been suggested in a recent paper [6]. Non-first-order reactions do add some complexity; however, the basic essence remains the same. The propene yield can be optimized with a proper choice of catalyst and operating conditions.

The use of phosphorous as a modifier for titania-supported vanadia catalyst or the more commonly expressed VPO/TiO_2 has been documented [8–13]. In the present study phosphorous is used as a modifier for a less-than-monolayer V_2O_5/TiO_2 catalyst to understand the effect on the rate constants for propane ODH reaction. The catalyst synthesized by the incipient-wetness impregnation technique is initially characterized for its surface area and by Raman spectroscopy and H_2 temperature-programmed reduction (TPR) studies. The propane ODH reaction over these catalysts is then considered, and the kinetic parameters are determined for a simplified Mars–van Krevelen (MVK) reaction mechanism. Based on the kinetic parameters determined, the effect of phosphorous on the kinetic parameters and the ratio of the rate constants is elaborated.

2. Experimental

2.1. Sample preparation

The unmodified and phosphorous-modified titania-supported vanadium oxide catalysts were prepared by the incipient-wetness impregnation method. The precursors used for vanadium and phosphorous were ammonium metavanadate (NH_4VO_3) and diammonium hydrogen phosphate [$(NH_4)_2HPO_4$], respectively. Initially, a large batch of the support was pretreated with an incipient-wetness volume of oxalic acid solution of a known concentration (0.1 g cc^{-1}). The support was then dried in a desiccator at room temperature for 12 h, followed by drying at 383 K in an oven for 12 h, and finally calcined in an electric furnace at 733 K for 12 h.

The incipient-wetness impregnation of vanadium and/or phosphorous of the above pretreated support was carried out with a solution containing the corresponding ions. A vanadium oxalate solution was initially prepared by the addition of known amounts of ammonium metavanadate with a stoichiometric amount of oxalic acid in water. To prepare the phosphorous-modified samples, diammonium hydrogen phosphate was added to the solution containing ammonium metavanadate and oxalic acid and stirred in water until the entire solid was dissolved. A deep blue solution was formed with and without phosphorous precursor, which was further diluted with double-distilled water in such a way that the total volume corresponded to the incipient-wetness impregnation volume of the support. The above solution was intimately mixed in a crucible with the pretreated support to form a paste. The paste was heat-treated in a manner similar to that described above for the pretreatment of the support.

In the present study four catalyst samples were prepared from the same pretreated TiO_2 support; they are listed in Table 1 in terms of their nomenclature and percentage weight of V_2O_5 and P_2O_5. Also listed in Table 1 are surface area values and results from TPR characterization studies, which are discussed later. Sample 1 contained 3 wt% vanadium oxide as V_2O_5 and is referred to as 3VTi. Sample 2 contained 3 wt% V_2O_5 and 1.2 wt% P_2O_5, with a V/P molar ratio of 2:1 and is referred to as 2V1PTi. Similarly, samples 3 and 4 contained 2.9 wt% V_2O_5 and 2.3 wt% P_2O_5, and 2.9 wt% V_2O_5 and 4.5 wt% P_2O_5, with V/P molar ratios of 1:1 and 2:1, and are referred to as 1V1PTi and 1V2PTi, respectively.

Table 1
Nomenclature, composition, surface area and H_2-TPR results of the samples

Sl. No.	Nomenclature	wt% of V_2O_5 in the sample	wt% of P_2O_5 in the sample	V:P molar ratio	V atoms (nm^{-2})	P atoms (nm^{-2})	Surface area ($m^2\,g^{-1}$)	H_2-TPR results	
								T_{max} (K)	H/V ratio
1	TiO_2	0.0	0.0	–	–	–	43	–	
2	3VTi	3.0	0.0	–	4.6	–	43	718	2.0
3	2V1PTi	3.0	1.2	2:1	4.7	2.4	42	751	1.6
4	1V1PTi	2.9	2.3	1:1	4.7	4.7	41	751	1.4
5	1V2PTi	2.9	4.5	1:2	4.6	9.1	41	778, 862	1.3

2.2. Characterization

The phosphorous-modified and unmodified VTi samples are characterized by their surface areas, Raman spectra, and TPR profiles.

2.2.1. Surface area studies

The surface areas of the catalyst samples were determined with a Coulter SA 3100 analyzer equipped with SA-View software, with N_2 as the adsorbate.

2.2.2. Raman spectroscopy

The in situ Raman spectra were run with a Renishaw Micro-Raman System 1000 equipped with a cooled CCD detector (200 K) and a holographic super-Notch filter that removes the elastic scattering. The samples were excited with the 514-nm Ar line in an in situ cell (Linkam, TS-1500), which allows temperature treatments up to 1773 K under flowing gases. The spectral resolution was 3 cm^{-1}, and the spectra acquisition consisted of five accumulations of 60 s for each sample. The spectra of the samples under dehydrated conditions were acquired at 423 K, and the spectra under ambient conditions where run with flowing humid air. The spectra of the TiO_2-supported samples were normalized based on the ∼635 cm^{-1} peak of bulk TiO_2 to facilitate comparison between the different samples.

2.2.3. Temperature-programmed reduction studies

The temperature-programmed reduction (TPR) experiments were performed in a Micromeritics Pulse Chemisorb 2705 apparatus. For this purpose 0.05 g of sample was placed in a quartz reactor. We pretreated the sample by heating it in a He gas flow (30 cc min^{-1}) to 423 K and then maintaining this temperature for 30 min. After cooling to 308 K, the sample was subsequently brought into contact with an H_2/Ar mixture (H_2/Ar volume ratio of 05:95 and total flow rate of 50 cc min^{-1}) and heated to a final temperature of 1230 K at a constant rate of 10 K min^{-1}. The hydrogen concentration of the exit gas was detected by a thermal conductivity detector.

2.3. Propane ODH reactivity studies

2.3.1. Reaction setup

All of the catalysts were tested for the ODH of propane in a fixed-bed, down-flow, tubular quartz reactor with a length of 300 mm, an inlet diameter of 10 mm, and an outlet diameter of 5 mm. The amount of catalyst was varied from 0.03 to 0.2 g, depending on the specific objective. Quartz powder was used as a diluent with the catalysts to prevent temperature gradients and to avoid channeling of gas within the catalyst bed. The catalyst bed containing the catalyst and quartz powder mixture was placed on the quartz wool at the center of the quartz reactor. The reactant mixture of C_3H_8 and air at a specified C_3H_8/O_2 molar ratio and total flow rate were controlled with two independent thermal mass flow controllers (Bronkhost Hi-Tech, model F201d FAC-22-V). Additional details of the reaction setup are given elsewhere [6].

With this reaction setup, data were collected to determine reproducibility, effect of contact time, and kinetic parameters.

2.3.2. Data for reproducibility studies

For this study two catalyst samples were chosen: 3VTi and 1V1PTi. For both samples, the C_3H_8/O_2 molar ratio was maintained at 1:1, and the total volumetric flow rate was 75 cc min^{-1}. The weights of 3VTi and 1V1PTi catalysts for the reproducibility studies were 0.05 and 0.10 g, respectively. Initially, the temperature was increased from 683 to 713 K at 20 K intervals. Subsequently, the temperature was reduced to 683 K by the same temperature intervals. At each temperature the reaction data were collected. Thus, the data were collected at 653, 673, 693, 713, 693, 673, and 653 K.

2.3.3. Data for contact time studies

For contact time studies over a particular catalyst, the temperature was kept constant at 643 K, the C_3H_8/O_2 molar ratio was maintained at 2:1, and the total volumetric flow rates were varied as 120, 90, 75, 45, 30, and 20 cc min^{-1}. Catalyst amounts ranged from 0.05 to 0.2 g to ensure that different catalysts were compared for constant contact time and/or constant conversion.

2.3.4. Data for kinetic parameter estimation studies

To obtain the data for kinetic parameter estimation, the C_3H_8/O_2 ratio was varied as 3:1, 2:1, and 1:1, and at each ratio the data were collected at 653, 673, 693, and 713 K. The total volumetric flow rate was maintained at 75 cc min^{-1}. The catalyst amounts, however, ranged from 0.03 to 0.2 g.

2.3.5. Reactivity calculations

The calculations of conversion, selectivity, yield, and carbon balance were based on the mole fractions determined from the GC peaks. The formulae for conversion, selectivity, yield, and carbon balance are given elsewhere [6,14].

2.3.6. Kinetic parameter estimation

To obtain the kinetic parameters, the reactor was subjected to integral analysis. Advantages of this method over conventional differential analysis are given in detail elsewhere [15]. Based on integral analysis, the differential material balance equation for each component, i, for a particular reaction network can be written as

$$V_0 y_i|_W - V_0 y_i|_{W+\mathrm{d}W} - \sum_j n_{ij} r_j \,\mathrm{d}W = 0, \quad i = 1, \ldots, v, \tag{1}$$

where

V_0 volumetric flow rate of the feed;
y_i mole fraction of the ith component;
n_{ij} stoichiometric coefficient of the ith component for the jth reaction given in Scheme 1;
r_j rate of jth reaction (a function of θ_j and x_i or $r_j = f_j(x_i, \theta_j)$);
θ_j kinetic parameters for the jth reaction;
v number of components;
W weight of the catalyst.

Simplification of Eq. (1) with the assumptions mentioned above results in

$$\frac{\mathrm{d}y_i}{\mathrm{d}W} = \sum_j n_{ij} r_j / V_0. \tag{2}$$

The set of ordinary differential equations represented in Eq. (2) can be solved to obtain the model-output mole fraction of each component based on the initial component mole fraction, y_{i0}, and W, n_{ij}, V_0, and r_j. The values of y_{i0}, W, n_{ij}, and V_0 are known, and the specific reaction rate, r_j, depends on the reaction mechanism considered. The reaction mechanism is characterized by several kinetic parameter, θ_j, which are nonlinear in nature, and some or all mole fractions, y_i. Thus, the output mole fraction is obtained by integration over the entire mass based on a chosen reaction mechanism. Integration over the entire mass is done with the Runga–Kutta fourth-order technique.

The response data, the output mole fraction of C_3H_8, C_3H_6, CO, and CO_2, are assumed to be well described by a nonlinear model given by

$$Y_h = g_h(\theta, x) + Z_h, \quad h = 1, 2, \ldots, v, \tag{3}$$

where

Y_h vector of random variables representing the response variable;
$g_h(\theta, x)$ predicted or model-output concentration;
θ parameter vector;
x concentration vector;
Z_h error associated with calculation of the response h.

The predicted output mole fraction for the ith component and uth experiment, $y_{iu,\mathrm{pred}}$, obtained in this way can then be compared with the actual output mole fraction y_{iu}. To obtain the best value of the parameters, minimization of an objective function is required.

2.3.7. Objective function

For multiresponse systems and when responses are correlated, the ideal criterion is the minimization of the determinant [16–20]:

$$\text{Determinant criteria for multiresponse systems} = \min |Z_{hk}|, \tag{4}$$

where

$$Z_{hk} = \sum_{u=1}^{n} (y_{hu} - g_{hu})(y_{ku} - g_{ku}); \tag{5}$$

h and $k = 1, \ldots, v$;

n no. of experiments;
v no. of responses;
y_{hu} experimental mole fraction of the hth component in the uth experiment;
g_{hu} predicted mole fraction of the hth component in the uth experiment.

In the present study the determinant criteria given by Eq. (4) are considered.

2.3.8. Genetic algorithm

Minimization of the objective function given by Eq. (4) is achieved by application of a genetic algorithm (GA). The GA source code is from the Kangal laboratory, IIT Kanpur, which was developed by Deb and co-workers [21]. The GA implementation in this study is restricted to real coded variables only. All constraints used in this code are greater-than-equal-to type ($g \geqslant 0$) and normalized. This general code was then modified according to the present study to obtain the kinetic parameters. Initially, a population of solution was randomly generated. The size of population was from 80 to 150 for the MVK model chosen, which is discussed later. The variable boundaries are fixed for each parameter, and boundaries are fixed according to previous knowledge of the parameters. Selection of parents from the pool of solutions is done by tournament selection. The size of tournament in the present study was 2. Crossover probability exchanges information among parent solutions, whereas the polynomial mutation operator is used to introduce extra diversity to the solutions. The values of crossover and mutation probability were 0.9 and 0.1, respectively. In the present study the parameters are real; thus simulated binary crossover (SBX) is considered. The exponents of SBX and mutation were 2 and

Table 2
GA parameters used in the present study

GA parameters	Values for MVK models
Generations	5000–50000
Population size	80–150
Crossover probability	0.9
Mutation probability	0.1
Tournament size	2
Exponent for simulated binary crossover	2
Exponent for mutation	200
Seed value	0.123–0.2

200, respectively. The termination criterion used in this GA code was the total number of generations. The number of generations was varied from 5000 to a maximum of 50000 to obtain stable solutions. All of the parameters used in the GA code are listed in Table 2.

2.3.9. Reaction model

The choice of the reaction model is important for kinetic analysis. For the purpose of understanding the structure–reactivity relationship for unmodified and phosphorous-modified VTi catalysts, a MVK mechanism is considered.

According to the MVK mechanism chosen for this study, the propane molecules react with lattice oxygen of the catalyst to produce propene molecules and carbon oxides. The gas-phase oxygen replenishes the lattice oxygen by reoxidation of the catalyst. Thus, there are four reactions considered: r_1, r_2, r_3, and r_{reox}. These four reactions are given below.

1. Formation of propene (r_1):
   Gas-phase propane reacts with lattice oxygen, forming gas-phase propene:

   $$C_3H_8(g) + O(s) \rightarrow C_3H_6(g) + H_2O + *_{\text{red}}, \quad (6)$$

   where $*_{\text{red}}$ is a reduced site.
2. Formation of CO from propene (r_2):
   Gas-phase propene reacts with lattice oxygen to form gas-phase CO:

   $$C_3H_6(g) + 6O(s) \rightarrow 3CO(g) + 3H_2O + 6*_{\text{red}}. \quad (7)$$

3. Formation of CO_2 from propene (r_3):
   Gas-phase propene reacts with lattice oxygen to form CO_2 gas:

   $$C_3H_6(g) + 9O(s) \rightarrow 3CO_2(g) + 3H_2O + 9*_{\text{red}}. \quad (8)$$

4. Reoxidation (r_{reox}):
   Finally, the catalyst is reoxidized by gas-phase oxygen:

   $$O_2 + 2*_{\text{red}} \rightarrow 2O(s). \quad (9)$$

   The reaction rates for the above four reactions, (6)–(9), are expressed as

   $$r_1 = k_1 P_{C_3H_8}(1-\beta), \quad (10)$$

   $$r_2 = k_2 P_{C_3H_6}(1-\beta), \quad (11)$$

   $$r_3 = k_3 P_{C_3H_6}(1-\beta), \quad (12)$$

   $$r_{\text{reox}} = k_4 P_{O_2}\beta, \quad (13)$$

   where k_j is the rate constant for the jth reaction, in ml STP min^{-1} $\text{g}_{\text{cat}}^{-1}$ atm^{-1}; P_i is the partial pressure of the component, i, in atm; and β is the degree of reduction of the catalyst, which is dimensionless.

Assuming that the rate of oxygen consumed in the reactions r_1, r_2, and r_3 is equal to the rate of oxygen replacement by the reaction r_{reox}, β can be expressed as

$$\beta = \frac{0.5k_1P_{C_3H_8} + 3.0k_2P_{C_3H_6} + 4.5k_3P_{C_3H_6}}{0.5k_1P_{C_3H_8} + 3.0k_2P_{C_3H_6} + 4.5k_3P_{C_3H_6} + k_4P_{O_2}}. \quad (14)$$

The justifications for using these four reactions are given elsewhere [6,14].

2.3.10. Reparameterization

Kinetic parameter estimates obtained by fitting of models to data are often highly correlated with each other. Under such circumstances the parameters are of little use for predicting the nature of the system [6]. In chemical kinetics high correlations are frequently encountered between estimates of the kinetic parameters in the Arrhenius expression for a rate constant, making the elucidation of a reaction network very difficult [22]. To decrease the correlation between parameters, reparameterization is required. Reparameterization is achieved by reformulating the rate constants as

$$k_i = k_{i0}\exp\left[-\frac{E_i}{R}\left(\frac{1}{T}-\frac{1}{T_m}\right)\right], \quad (15)$$

where

k_{i0} the pre-exponential factor (ml STP min^{-1} $\text{g}_{\text{cat}}^{-1}$ atm^{-1});
E_i the activation energy for the reaction i (kJ/mol);
T the actual reaction temperature (K);
R the universal gas constant (kJ kmol^{-1} K^{-1}); and
T_m is the mean temperature (K).

This type of centering reduces the correlation between the activation energy and the pre-exponential factor [22,23].

2.3.11. Standard error calculation

Standard error calculation provides a measure of accuracy associated with the estimation of kinetic parameters. For standard error calculation, a Bayesian criterion was followed in which it was assumed that the each row of Z follows a multivariate normal distribution [24]. Accordingly, the standard error $\text{se}(\hat{\theta}_p)$ for the kinetic parameters, θ_p, is then given by

$$\text{se}(\hat{\theta}_p) = \left\{\left(2s^2\Gamma^{-1}\right)_{pp}\right\}^{0.5}, \quad (16)$$

where $2s^2\Gamma^{-1}$ is the covariance matrix $\hat{\theta}$. The value of s^2 is obtained by dividing the determinant value at optimized

conditions by the degrees of freedom $N - P$, where N is the number of experiments and P is the number of kinetic parameters. Furthermore, Γ is an approximate Hessian of $|Z^{\mathrm{T}}Z|$ calculated at the optimized kinetic parameter values.

3. Results and discussion

Initially, the characterization results are presented, which are followed by the results of the propane ODH reaction.

3.1. Characterization studies

3.1.1. Surface area studies

The surface areas of pure titania (TiO_2), 3% V_2O_5/TiO_2, and phosphorous-modified V_2O_5/TiO_2 were obtained and tabulated in the eighth column of Table 1. The surface area values for all of the samples are relatively constant, varying between 41 and 43 $m^2\,g^{-1}$. Consequently, it appears that the support is not significantly affected during preparation of the catalysts. Other researchers have also observed similar variations in surface area [12,25–27]. Two P_2O_5/TiO_2 samples, 1 and 4.6%, had surface area values of 47 and 41 $m^2\,g^{-1}$, respectively [28].

3.1.2. Raman studies

The Raman spectra of the unmodified and modified V_2O_5/TiO_2 samples obtained under dehydrated conditions are shown in Fig. 1. The ∼635 cm^{-1} TiO_2 Raman peak used for normalization is not shown for clarity. The broad Raman feature at 790 cm^{-1} is due to the TiO_2 support. The unmodified 3VTi sample reveals a broad band at ∼900 cm^{-1} and a sharper band at 1020 cm^{-1}. These Raman bands are due to the surface vanadia species present on the titania support. With an increase in phosphorous content, the intensities of the two Raman bands due to the surface vanadia species decrease and broaden, except for the sample with the highest phosphorous content, 1V2PTi. For the 1V2PTi sample two relatively sharp Raman bands are observed at 925 and 1037 cm^{-1}, suggesting that a different vanadia species is formed. These two bands are not sensitive to hydration-dehydration conditions. Similar Raman bands are observed at 923 and 1035 cm^{-1} for a 3% P_2O_5/1% V_2O_5/TiO_2 sample [8] and for a post-reaction sample of vanadia supported on α-titanium phosphate [11]. These Raman bands at ∼925 and ∼1035 cm^{-1} closely correspond to the bands of α_I-$VOPO_4$ [29]. Interestingly, the 3% P_2O_5/1% V_2O_5/TiO_2 sample was prepared by sequential preparation, whereas the present 1V2PTi samples was prepared by co-precipitation. Furthermore, XRD spectra for the different phosphorous-modified and unmodified 3% V_2O_5/TiO_2 samples do not reveal any features other than those of the TiO_2 support [28]. Thus, the 1V2PTi sample possesses nanosized α_I-$VOPO_4$ that is not detected by XRD.

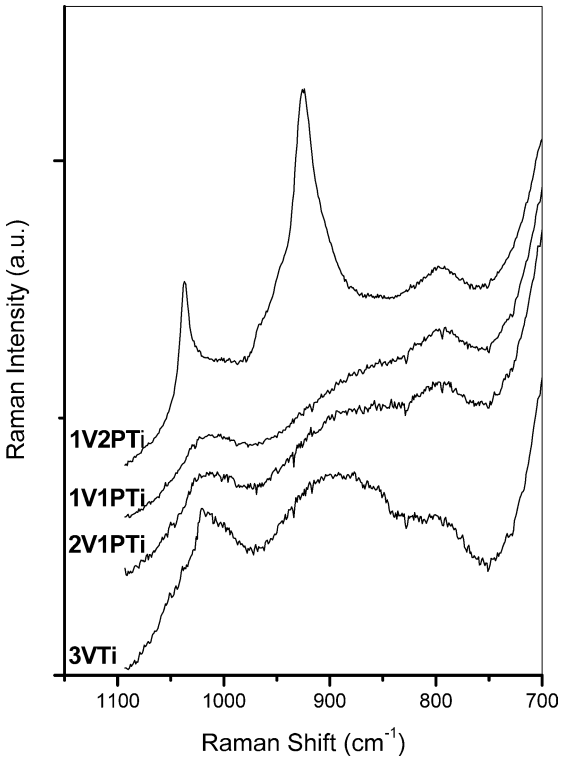

Fig. 1. Raman spectra obtained under dehydrated conditions of VTi and phosphorous-modified VTi samples.

3.1.3. Temperature-programmed reduction studies

TPR profiles for the modified and unmodified V_2O_5/TiO_2 samples were obtained. The TPR profiles of the TiO_2 support did not show any features in the temperature range considered [28]. A single T_{max} was observed for all vanadium oxide-containing samples, except for 1V2PTi, for which two reduction peaks are observed. The presence of a different TPR profile for the 1V2PTi sample is consistent with the Raman studies that reveal the presence of α_I-$VOPO_4$ species in the sample. The T_{max} temperatures for the four samples are listed in the ninth column of Table 1. From the data presented in the ninth column of Table 1 it is observed that the T_{max} temperature of the first reduction peak increased from 718 to 751 K for 2V1PTi and 1V1PTi. The 1V2PTi sample exhibits two reduction peaks at higher temperatures (778 and 862 K). A weak, broad reduction peak is observed for vanadium-free 1.2% P_2O_5/TiO_2 at 820 K, suggesting that the T_{max} temperatures listed in Table 1 are due to vanadia or vanadia–phosphorous interactions [28].

For quantitative analysis, the first reduction peak areas were integrated to determine the amount of hydrogen consumed. The hydrogen consumed per vanadium atom present in the sample was determined and the H/V atomic ratio was calculated. The H/V values are listed in the tenth column of Table 1. It can be observed that the H/V atomic ratio is 2.0 for 3VTi, indicating the reduction of V^{5+} to V^{3+}. The H/V value decreased nonlinearly with an increase in phosphorous content for the modified catalysts. Similar TPR results showing the affect of phosphorous modification have also been

observed before [25,30]. The decrease in the H/V ratio that occurs with an increase in phosphorous content is consistent with the decrease in the Raman bands due to the surface vanadia species.

The higher T_{max} values that occur with increasing phosphorous content suggest that the vanadia sites are less reducible. Furthermore, the H/V ratio ranging from 1.3 to 1.6 for the phosphorous-modified VTi samples suggests the presence of both V^{5+} and V^{4+} in the fresh samples. In addition, the decrease in the H/V ratio suggests that decreasing amounts of V^{5+} species are present. Indeed, the EPR spectra reveal an increase in V^{4+} species [28]. Taking into account the Raman, TPR, and EPR studies, it appears that part of the V^{5+} is converted to V^{4+} oxide species. The broadening of the V=O mode intensity in 2V1PTi and 1V1PTi would be indicative of an interaction between surface V and P oxide species. The V–P interaction would account for stabilization of some V^{4+} sites (similar to some VPO phases) [29] and for the lower reducibility. The 1V2PTi sample behaves differently, since V–P interaction leads to α_I-$VOPO_4$. There is an additional difference in the 1V2PTi catalyst. The P + V coverage, expressed as (P + V) atoms nm^{-2} of the titania support, was 7, 9, and 13 for 2V1PTi, 1V1PTi, and 2V1PTi, respectively. Thus, the total P + V coverage was above a monolayer in 1V2PTi, with 13 (P + V) atoms nm^{-2} (dispersion limit is near 9 atoms nm^{-2}). Other supported binary systems show that no bulk tridimensional structure forms if the total coverage is below the dispersion limit, such as Sb + V supported on alumina [31] on zirconia [32], or for alumina-supported Mo + V [33]. This also appears to be the case for P + V on titania. Below the P + V dispersion limit no bulk VPO phase forms; however, there is evidence for surface vanadium and surface phosphorous oxide interactions.

3.2. Reactivity studies

The propane ODH reaction was carried out over the 3VTi and phosphorous-modified VTi catalysts to obtain data for reproducibility studies, contact time effects, and kinetic parameter estimation.

3.2.1. Data for reproducibility studies

Two catalysts, 3VTi and 1V1PTi, were chosen to determine the reproducibility of the reaction data. Results obtained for 1V1PTi are shown in Fig. 2. In this figure the C_3H_6, CO, and CO_2 yields were plotted as the temperature was initially increased and then decreased. Arrows show the temperature trends. From Fig. 2 it is observed that the yields are essentially independent of the temperature history. Similar reproducibility data are achieved for the 3VTi sample [28]. Consequently, the reaction data appear to be reproducible in the operating conditions considered in the present study.

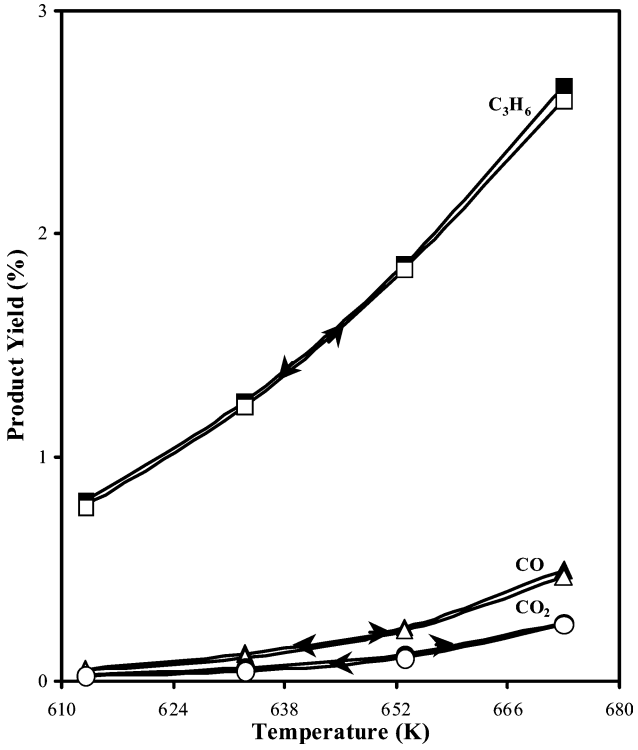

Fig. 2. Product yield versus temperature for 1V1PTi sample showing the reproducibility of propane ODH. Total flow rate = 75 ml min^{-1}; C_3H_6:O_2 = 1:1; weight of the catalyst = 0.10 g.

3.2.2. Data for contact time studies

To analyze the effect of contact time, the propane ODH reaction was performed over the four ODH active catalyst samples at different contact times. The C_3H_8/O_2 ratio was maintained at 2:1 and the temperature at 643 K. It was observed that the conversion increased with an increase in contact time. Furthermore, at the same contact time the conversion decreased with an increase in phosphorous content in the catalyst. For example, at a contact time of 67 (kg m^{-3} s) the conversion for 3VTi was the highest, 2.3%, followed by 2V1PTi (1.7%), 1V1PTi (1.1%), and finally 1V2PTi (0.5%). Thus, in terms of activity, 3VTi > 2V1PTi > 1V1PTi > 1V2PTi.

The propene selectivity variation with respect to the propane conversion for the different catalysts reveals that the conversion and propene selectivity are inversely related. Furthermore, the selectivity at iso-conversion increases as the phosphorous content in the catalyst increases. For example, at 2.3% propane conversion the propene selectivities are 72% for 3VTi, 81% for 2V1PTi, 82% for 1V1PTi, and 86% for 1V2PTi. Consequently, the propene yield or selectivity at iso-conversion follows the trend 1V2PTi > 1V1PTi $\geqslant$ 2V1PTi > 3VTi. This trend in selectivity parallels the structural changes observed by Raman spectroscopy and TPR studies. The incipient V–P interaction in 2V1PTi results in a better conversion–selectivity profile compared with the 3VTi, 2V1PTi, and 1V2PTi samples. Ciambelli et al. [12]

observed similar results during a contact time study for the ODH of ethane.

3.2.3. Data for kinetic parameter estimation

For each catalyst propane ODH reaction data were collected as a function of temperature (613, 633, 653, and 673 K) and C_3H_8/O_2 ratio (1:1, 2:1, and 3:1). Thus, reaction data were obtained under the 12 experimental conditions for each catalyst. Based on the data, the following ranges of product yields were observed:

C_3H_6 yield (%): 0.4–2.3,
CO yield (%): 0.01–0.41,
CO_2 yield (%): 0.01–0.22.

The salient features observed are:

1. The carbon balances (C_{in}/C_{out}) are greater than 0.95.
2. The C_3H_6, CO, and CO_2 yields decrease with an increase in C_3H_8/O_2 molar ratio, suggesting that oxidized conditions are beneficial for increasing the yields. Similar conclusions were obtained by Gao et al. for V_2O_5/ZrO_2 catalysts [34].
3. Comparison of the different yields at a particular C_3H_8/O_2 molar ratio with increasing temperature reveals that all of the yields increase, suggesting that temperature is also beneficial for increasing the yields.

A comparison of the different catalysts is not straightforward, since different catalyst amounts have been considered. A more general comparison is possible once the kinetic parameters are estimated. For example, once the kinetic parameters are estimated, comparison at equal contact time and iso-conversion is feasible.

3.2.4. Kinetic parameter estimation

Based on the input and output mole fractions, the kinetic parameters for the MVK model are determined by minimization of the objective function given by Eq. (4).

3.2.5. Predicted concentration

The predicted concentration values of C_3H_8, C_3H_6, CO_2, and CO under the 12 experimental conditions were calculated with the use of the kinetic parameters obtained for the four catalysts. Since the concentration of unreacted C_3H_8 was large in comparison with C_3H_6, CO, and CO_2, the predicted and actual concentrations were first normalized based on the highest concentration values. The normalized predicted versus actual concentrations are plotted in Fig. 3 for the MVK model. Fig. 3 reveals that there is a close correspondence between the predicted and actual concentrations of all observable carbon-containing compounds. Consequently, the kinetic parameters properly represent the steady-state reaction data.

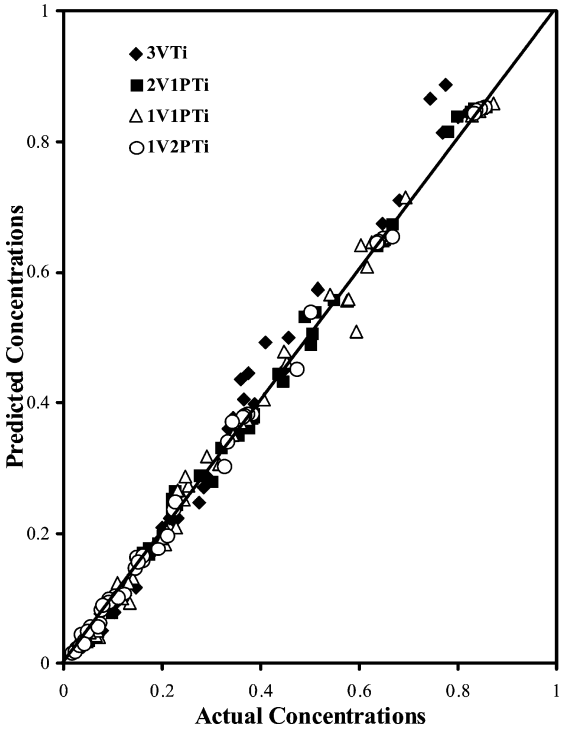

Fig. 3. Normalized predicted concentration versus normalized actual concentration for MVK model for VTi and phosphorous-modified VTi samples.

Table 3
Kinetic parameters for the four catalysts following MVK model[a]

Parameter	Units	Kinetic-parameter values for the catalyst			
		3VTi (S.E.)	2V1PTi (S.E.)	1V1PTi (S.E.)	1V2PTi (S.E.)
k_{10}	ml STP min^{-1} g_{cat}^{-1} atm^{-1}	34 (0.28)	29 (0.30)	14 (0.22)	4 (0.18)
k_{20}	ml STP min^{-1} g_{cat}^{-1} atm^{-1}	357 (3)	204 (21)	92 (2)	18 (1)
k_{30}	ml STP min^{-1} g_{cat}^{-1} atm^{-1}	328 (3)	196 (2)	84 (1)	17 (1)
k_{40}	ml STP min^{-1} g_{cat}^{-1} atm^{-1}	874 (61)	150 (5)	52 (2)	28 (4)
E_1	kJ mol^{-1}	81 (1)	79 (1)	70 (1)	69 (2)
E_2	kJ mol^{-1}	51 (1)	51 (1)	44 (2)	30 (3)
E_3	kJ mol^{-1}	45 (1)	52 (1)	44 (1)	33 (3)
E_4	kJ mol^{-1}	154 (5)	123 (3)	137 (3)	83 (9)

[a] $T_m = 643.16$ K, S.E. = standard error.

3.2.6. MVK model

The MVK model discussed above is based on a reaction scheme where propene is the primary product and CO and CO_2 are considered to be secondary products. It has eight kinetic parameters: four pre-exponential factors, k_{i0}, and four activation energies, E_i. The eight kinetic parameters for each catalyst were calculated at the mean reaction temperature, T_m, of 643 K; these are listed in Table 3. This table contains

six columns: in the first column lists the kinetic parameters, the second column lists the units of these kinetic parameters, and the third to sixth columns list the values of these parameters along with the standard error values in parentheses for the four catalysts.

Examination of the standard error relative to the kinetic parameter values in Table 3 suggests that the parameters are determined with a significant degree of accuracy. All pre-exponential factors, k_{i0}, decrease with an increase in phosphorous content in the sample. However, the activation energies, E_i, are relatively constant for the 3VTi, 2V1PTi, and 1V1PTi catalysts. For the 1V2PTi catalyst, the sample with the highest P content, the activation energies are significantly lower than those of the other catalysts. Furthermore, for each catalyst the k_{20} and k_{30} values are similar, and, along with the similarities of the activation energies, E_2 and E_3, it appears that the sites responsible for carbon oxide formation are similar.

Analysis of the kinetic parameters obtained for the four catalysts suggests that with an increase in phosphorous content, the pre-exponential factors, k_{i0}, gradually decrease, suggesting that the sites involved with these reactions are progressively poisoned. The decrease in sites is consistent with the Raman and TPR studies, in which the surface reducible vanadia species were found to decrease with an increase in phosphorous content in the sample. However, the surface vanadia may not be the only sites responsible for reactions r_1 to r_3 given by Eqs. (10)–(12). To observe the relative decrease in the k_{i0} values, the pre-exponential factors for each catalyst normalized with the pre-exponential factor for 3VTi, $(k_{i0})_{\text{normalized}}$, are plotted in Fig. 4. Fig. 4 reveals that the k_{i0} values decrease with an increase in phosphorous content at different rates: the k_{20} and k_{30} values decrease more rapidly in comparison with the decrease in k_{10} values, and the k_{40} value decreases the most rapidly among all of the pre-exponential factors. Thus, the relative poisoning of the sites responsible for the r_1 to r_3 and r_{reox} reactions varies.

The pre-exponential factor is usually associated with the number of active sites or the activity per site [35]. Consequently, with an increase in phosphorous content there is a decrease in the number of active sites, the activity per site, or both. Comparison of the three activation energy values for the 3VTi, 2V1PTi, and 1V1PTi catalysts given by the mechanistic MVK model suggests that the catalytic cycles involved in reactions r_1 to r_3 and r_{reox} are similar for these three catalysts. The 1V2PTi sample shows different E_i values, suggesting that a different species is involved. This is consistent with the Raman and TPR studies, since a new species is formed that possesses a distinctly different reduction profile.

Variation of the degree of reduction, β, given by the MVK model is also calculated by Eq. (14) for the unmodified and phosphorous-modified VTi catalysts. It is observed that the degree of reduction increases with an increase in propane conversion [28]. At iso-conversion values (<5%) the degree of reduction is the same for all of the catalysts. At high conversion values, however, the degree of reduction follows the trend 3VTi > 2V1PTi > 1V1PTi > 1V2PTi. Thus, at low conversions the ratio of oxidized and reduced sites to the total number of sites is the same for the unmodified and phosphorous-modified VTi catalysts, but at high conversions the fraction of reduced sites is the most for the 3VTi and lowest for the 1V2PTi catalyst.

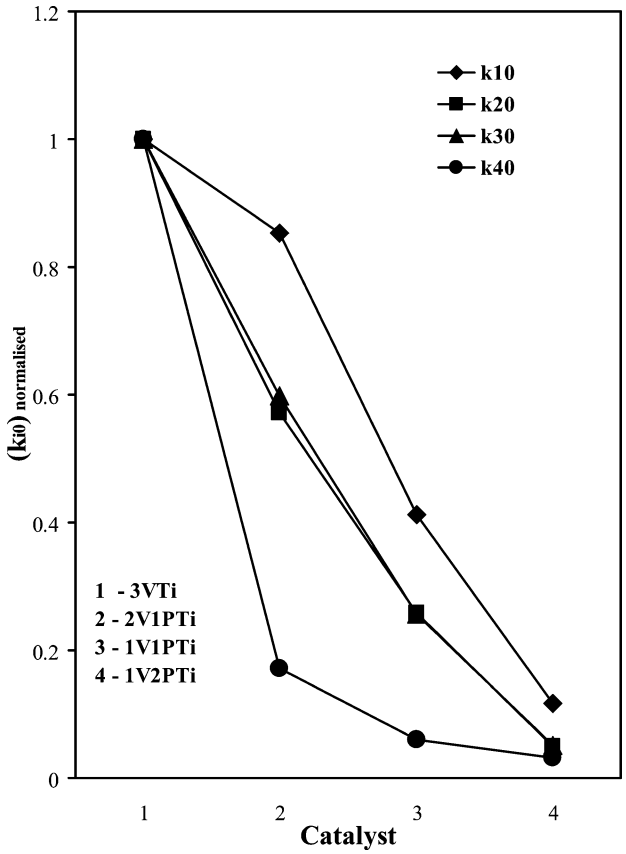

Fig. 4. Normalized pre-exponential factor for different catalysts using MVK model.

The kinetic parameters can also be used for catalyst design and development, since the rate constants k_i depend on the values of k_{i0} and E_i and the temperature of the reaction. The rate constant k_1 is related to the desirable propane ODH reaction, and the rate constants k_2 and k_3 are related to the undesirable propene degradation reaction. For a consecutive reaction mechanism, as in the MVK model chosen here, the propene yield depends on the contact time and the $(k_2 + k_3)/k_1$ value [6,7]. At a particular temperature, as the contact time increases the propene yield initially increases and then decreases. The yield at a specific contact time is a function of the $(k_2 + k_3)/k_1$ ratio. For a particular catalyst the $(k_2 + k_3)/k_1$ ratio can be changed by a change in the temperature. For example, in the present study the $(k_2 + k_3)/k_1$ ratio decreases with an increase in temperature. Consequently, the contact time where the propene yield is optimum is also a function of temperature. This is clearly shown in Fig. 5, where the predicted propene yield for the 3VTi catalyst is plotted versus the contact time for different

$(k_2+k_3)/k_1$ values corresponding to different temperatures. It is observed that oxygen is depleted before the propene yield reaches a maximum for the net reducing environment considered. Consequently, the optimum contact time cannot be determined. Comparing the propene yield at a particular contact time suggests that the propene yield increases as the $(k_2+k_3)/k_1$ decreases or the reaction temperature increases. The dominating factor affecting the change in the $(k_2+k_3)/k_1$ ratio is the difference in the activation energies between the propene formation and propene degradation reactions. Similar plots are observed for the other catalysts. Thus, the reaction can be conducted at the proper contact time for achieving maximum propene yield at a particular temperature. Furthermore, the maximum propene yield can also be improved by the use of higher temperatures.

The above analysis suggests that a proper $(k_2+k_3)/k_1$ ratio is critical in improving the propene yield. The change in the ratio arises from the relative change in the rate constants associated with the propene degradation and propene formation reaction. A change in $(k_2+k_3)/k_1$ can be achieved by a change in the temperature, as shown above, or by a change in the catalyst composition. In Fig. 6, the predicted propene yield is plotted versus propane conversion for the four catalysts. The temperature was fixed at 643 K and the C_3H_8/O_2 ratio was 2:1. Fig. 6 reveals that at a particular propane conversion, the propene yield also increases with a decrease in $(k_2+k_3)/k_1$. The decrease in $(k_2+k_3)/k_1$ is achieved here by an increase in the phosphorous content. Consequently, by the choice of the appropriate catalyst, the propene yield can also be increased. The dominant factor for a changing catalyst at a specific temperature is the change in the pre-exponential factor ratios, $(k_{20}+k_{30})/k_{10}$. The analysis above also confirms the contact time results, where the selectivity increases with phosphorous addition at iso-conversion levels [28]. Fig. 6 also reveals that the predicted propene yield monotonically increases and before or near the point where the optima oxygen is depleted. Furthermore, the propene yields given by the MVK model in Fig. 6 are similar for the 2V1PTi and 1V1PTi catalysts, which is consistent with the contact time results [28].

In Fig. 7 the propene selectivity is plotted versus propane conversion. Fig. 7 reveals that the propene selectivity and propane conversion are inversely related, and at iso-conversion the maximum propene selectivity is observed for the 1V2PTi catalyst, whereas the least propene selectivity is ob-

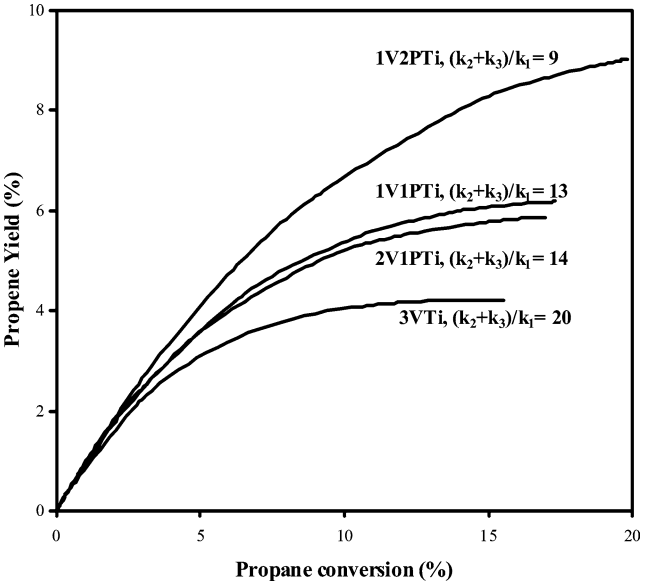

Fig. 6. Predicted propene yield versus propane conversion for VTi and phosphorous-modified VTi samples. Temperature = 643 K; C_3H_6:O_2 = 2:1; weight of the catalysts = 1.00 g.

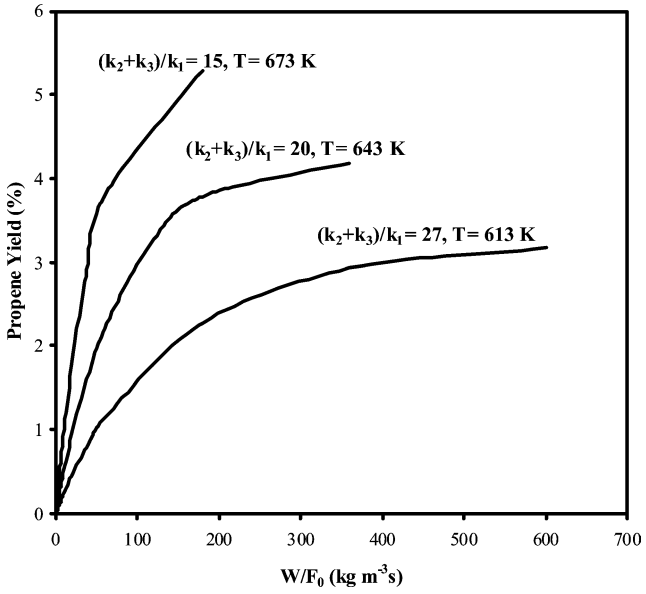

Fig. 5. Predicted propene yield versus contact time for 3VTi catalyst. Weight of the catalyst = 0.03 g; C_3H_6:O_2 = 2:1.

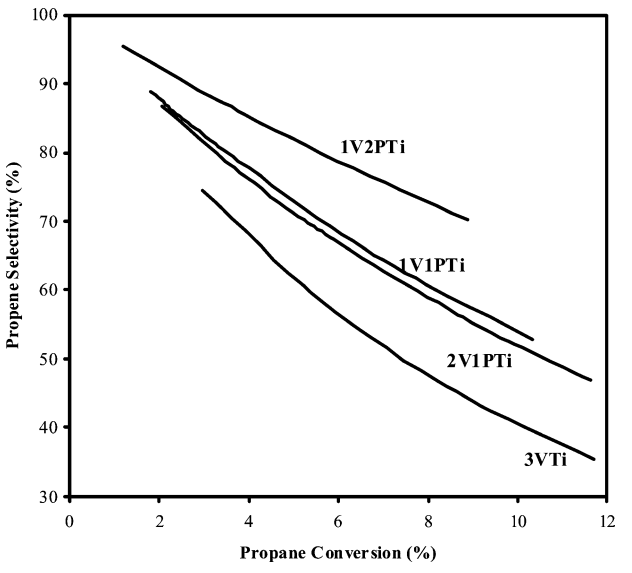

Fig. 7. Predicted propene selectivity versus propane conversion for VTi and phosphorous-modified VTi samples. Temperature = 643 K; C_3H_6:O_2 = 2:1; weight of the catalysts = 1.00 g.

served for the 3VTi catalyst. Furthermore, the propene selectivities for the MVK model are similar for the 2V1PTi and 1V1PTi catalysts, which is consistent with the characterization and reaction studies. Fig. 7 also reveals that it is possible to fine-tune the inverse conversion-selectivity relationship with the help of phosphorous.

4. Conclusions

V–P–O/TiO_2 catalysts with varying V/P ratios were synthesized and characterized by various techniques. No significant change in surface area was observed, suggesting that the support was not affected during preparation. Raman spectra of the catalysts reveal two scenarios: when the V + P loading is above the dispersion limit, nanoscale VPO phases (α_I-$VOPO_4$) form, whereas the V–P interaction between the surface V and surface P species is evident at lower coverages. The TPR profiles reveal an increase in the V^{4+}/V^{5+} ratio with P/V atomic ratio. A new reduction profile is evident when the V + P coverage is above a monolayer, where α_I-$VOPO_4$ forms. The TPR profile also suggests that the reducibility of the surface V^{5+} species is affected, since the T_{max} temperature increases with phosphorous content. The propane ODH reaction revealed that the conversion and selectivity are inversely related for all catalysts. At constant contact time the conversion decreased with increasing phosphorous content. At iso-conversions, however, the propene selectivity and yield increase with phosphorous content. This trend parallels the progressive interaction between P and V species.

The kinetic parameters were successfully estimated for a MVK model by minimization of an appropriate chosen determinant. Minimization is achieved by the application of a genetic algorithm. With the use of the kinetic parameters, the effect of phosphorous modification was explained. With an increase in phosphorous content, the pre-exponential factors progressively decrease, and, thus, the conversion decreases. The relative decrease varies for the different pre-exponential factors, however. The increase in propene yield at iso-conversion with an increase in temperature and phosphorous modification is due to the decrease in the ratio of rate constants due to propene degradation to propene formation, $(k_2 + k_3)/k_1$. The decrease in $(k_2 + k_3)/k_1$ ratio with phosphorous addition is primarily due to the dissimilar decrease in pre-exponential factors. Thus, with the proper design of the chemical constituents of the catalysts and under the proper operating conditions, the propene yield may be increased.

Acknowledgments

R.P.S. and G.D. are grateful for the financial assistance provided by the Ministry of Human Resources and Development (MHRD), India. M.A.B. is grateful for the financial assistance provided by the Spanish Ministry of Science and Technology (MAT-2002-0400-C02-01).

References

[1] E.A. Mamedov, V.C. Corberan, Appl. Catal. A 127 (1995) 1.
[2] F.D. Hardcastle, I.E. Wachs, J. Mol. Catal. 46 (1988) 173.
[3] G. Deo, I.E. Wachs, J. Haber, Crit. Rev. Surf. Chem. 4 (3/4) (1994) 141.
[4] I.E. Wachs, B.M. Weckhuysen, Appl. Catal. A 157 (1997) 67.
[5] A. Khodakov, B. Olthof, A.T. Bell, E. Iglesia, J. Catal. 181 (1999) 205.
[6] K. Routray, G. Deo, AIChE J. (2005), in press.
[7] H.S. Fogler, Elements of Chemical Reaction Engineering, second ed., Prentice-Hall of India Pvt. Ltd., New Delhi, 2003.
[8] G. Deo, I.E. Wachs, J. Catal. 146 (1994) 335.
[9] R.A. Overbeek, E.J. Bosma, D.W.H. de Blauw, A.J. van Dillen, H.G. Bruil, J.W. Geus, Appl. Catal. A: Gen. 163 (1–2) (1997) 129–144.
[10] I.E. Wachs, J.-M. Jehng, G. Deo, B.M. Weckhuysen, V.V. Guliants, J.B. Benziger, S. Sundaresan, J. Catal. 170 (1997) 75.
[11] J. Santamaría-González, M. Martínez-Lara, M.A. Bañares, M.V. Martínez-Huerta, E. Rodríguez-Castellón, J.L.G. Fierro, A. Jiménez-López, J. Catal. 181 (1999) 280.
[12] P. Ciambelli, P. Galli, L. Lisi, M.A. Massucci, P. Patrono, R. Pirone, G. Ruoppolo, G. Russo, Appl. Catal. A: Gen. 203 (1) (2000) 133.
[13] L. Lisi, P. Patrono, G. Ruoppolo, J. Mol. Catal. A: Chem. 204–205 (2003) 609.
[14] K. Routray, K.R.S.K. Reddy, G. Deo, Appl. Catal. A: Gen. 265 (1) (2004) 103.
[15] K.R.S.K. Reddy, M. Tech. Thesis, IIT Kanpur (2002).
[16] G.E.P. Box, N.R. Draper, Biometrika 52 (1965) 355.
[17] S. Vajda, P. Valko, Comp. Chem. Eng. 10 (1) (1986) 49.
[18] R. Mezaki, J.B. Butt, I & EC Fundamentals 7 (1) (1968) 120.
[19] G.F. Froment, K.B. Bischoff, Chemical Reactor Analysis and Design, second ed., Wiley, New York, 1990.
[20] G.E.P. Box, W.G. Hunter, J.F. MacGregor, J. Erjavec, Technometrics 15 (1) (1973) 33.
[21] Kangal: http://www.iitk.ac.in/kangal/soft.htm.
[22] D.G. Watts, Can. J. Chem. Eng. 72 (1994) 701.
[23] D.J. Pritchard, D.W. Bacon, Chem. Eng. Sci. 33 (1978) 1539.
[24] G. Kang, D.M. Bates, Biometrika 77 (1990) 321.
[25] R.A. Overbeek, P.A. Warringa, M.J.D. Crombag, L.M. Visser, A.J. van Dillen, J.W. Geus, Appl. Catal. A 135 (1996) 209.
[26] P. Ciambelli, L. Lisi, P. Patrono, G. Ruoppolo, G. Russo, Catal. Lett. 82 (2002) 243.
[27] L. Lisi, P. Patrono, G. Ruoppolo, Catal. Lett. 72 (2001) 207.
[28] R.P. Singh, M. Tech. Thesis, IIT Kanpur (2004).
[29] F. Ben Abdelouahab, R. Olier, N. Guilhaume, F. Lefebvre, J.C. Volta, J. Catal. 134 (1992) 151.
[30] L. Savary, J. Saussey, G. Costentin, M.M. Bettahar, M. Gubelmann-Bonneau, J.C. Lavalley, Catal. Today 32 (1996) 57.
[31] M.O. Guerrero-Pérez, J.L.G. Fierro, M.A. Vicente, M.A. Bañares, J. Catal. 206 (2002) 339.
[32] C.L. Pieck, M.A. Bañares, J.L.G. Fierro, Chem. Mater. 13 (2001) 1174.
[33] M.A. Bañares, S.J. Khatib, Catal. Today 96 (2004) 251.
[34] X. Gao, M.A. Bañares, I.E. Wachs, J. Catal. 188 (1999) 325.
[35] G. Deo, I.E. Wachs, J. Catal. 146 (1994) 323.